Inorg. Chem. **2005**, *44*, 6939–6948

Magnetic Properties of Cyano-Bridged Ln^{3+}–M^{3+} Complexes. Part I: Trinuclear Complexes (Ln^{3+} = La, Ce, Pr, Nd, Sm; M^{3+} = Fe_{LS}, Co) with bpy as Blocking Ligand

Albert Figuerola,[†] Joan Ribas,[†] Miquel Llunell,[†] David Casanova,[†] Miguel Maestro,[‡] Santiago Alvarez,*[,†] and Carmen Diaz*[,†]

Departament de Química Inorgànica, Universitat de Barcelona, Martí i Franquès, 1-11, 08028 Barcelona, Spain, and Departamento de Química Fundamental, Facultade de Ciencias, Universidade da Coruña,15071 A Coruña, Spain

Received April 27, 2005

The reaction of $Ln(NO_3)_{3(aq)}$ with $K_3[Fe(CN)_6]$ or $K_3[Co(CN)_6]$ and 2,2′-bipyridine in water/ethanol led to eight trinuclear complexes: *trans*-$[M(CN)_4(\mu\text{-}CN)_2\{Ln(H_2O)_4(bpy)_2\}_2][M(CN)_6]\cdot 8H_2O$ (M = Fe^{3+} or Co^{3+}, Ln = La^{3+}, Ce^{3+}, Pr^{3+}, Nd^{3+}, and Sm^{3+}). The structures for the eight complexes [La_2Fe] (**1**), [Ce_2Fe] (**2**), [Pr_2Fe] (**3**), [Nd_2Fe] (**4**), [Ce_2Co] (**5**), [Pr_2Co] (**6**), [Nd_2Co] (**7**), and [Sm_2Co] (**8**) have been solved; they crystallize in the triclinic space group $P\bar{1}$ and are isomorphous. They exhibit a supramolecular 3D architecture through hydrogen bonding and π–π stacking interactions. A stereochemical study of the nine-vertex polyhedra of the lanthanide ions, based on continuous shape measures, is presented. No significant magnetic interaction was found between the lanthanide(III) and the iron(III) ions.

Introduction

The design of supramolecular architectures with novel spin carrier topologies is of current interest in the field of molecular magnetism. A successful strategy leading to heteropolymetallic systems with extended structures consists of self-assembly processes involving anionic building blocks, which contain a paramagnetic ion, and assembling complex cations with potentially free coordination sites. Cyano-bridged bimetallic systems with interesting magnetic and photomagnetic properties have been characterized.[1] Most of these systems contain two different transition metal ions. In contrast, the lanthanide cations have been less used as nodes for the construction of cyano-bridged heteropolymetallic coordination networks.[2] Thus, although the research on cyano-bridged complexes has mainly focused on transition metal ions, with polycyanometalates and 4f ions, several compounds with differing dimensionality have been reported.[3−19] Focusing on trinuclear polycyanometalates complexes, only two systems have been reported containing

* To whom correspondence should be addressed. E-mail: carme.diaz@qi.ub.es.
[†] Universitat de Barcelona.
[‡] Universidade da Coruña.

(1) (a) Marvaud, V.; Decroix, C.; Scuiller, A.; Guyard-Duhayon, C.; Vaissermann, J.; Gonnet, F.; Verdaguer, M. *Chem. Eur. J.* **2003**, *9*, 1677 and references therein. (b) Ohba, M.; Ōkawa, H. *Coord. Chem. Rev.* **2000**, *198*, 313. (c) Verdaguer, M.; Bleuzen, A.; Marvaud, V.; Vaissermann, J.; Seuleiman, M.; Desplanches, C.; Scuiller, A.; Train, C.; Garde, R.; Gelly, G.; Lomenech, C.; Rosenman, I.; Veillet, P.; Cartier, C.; Villain, F. *Coord. Chem. Rev.* **1999**, *190*−*192*, 1023.
(2) (a) Benelli, C.; Gatteschi, D. *Chem. Rev.* **2002**, *102*, 2369. (b) de Sá, G. F.; Malta, O. P.; de Mello Donegá, C.; Simas, A. M.; Longo, R. L.; Santacruz, P. A.; da Silva, E. F., Jr. *Coord. Chem. Rev.* **2000**, *196*, 165.
(3) (a) Huliger, F.; Landolt, M.; Vetsch, H. *J. Solid State Chem.* **1976**, *18*, 307. (b) Huliger, F.; Landolt, M.; Vetsch, H. *J. Solid State Chem.* **1976**, *18*, 283.
(4) (a) Figuerola, A.; Diaz, C.; Ribas, J.; Tangoulis, V.; Granell, J.; Lloret, F.; Mahía, J.; Maestro, M. *Inorg. Chem.* **2003**, *42*, 641. (b) Figuerola, A.; Diaz, C.; Ribas, J.; Tangoulis, V.; Sangregorio, C.; Gatteschi, D.; Maestro, M, Mahía, J. *Inorg. Chem.* **2003**, *42*, 5274. (c) Figuerola, A.; Diaz, C.; El Fallah, M. S.; Ribas, J.; Maestro, M.; Mahía, J. *Chem Commun.* **2001**, 1204.
(5) Kou, H. Z.; Gao, S.; Jin, X. *Inorg. Chem.* **2001**, *40*, 6295.
(6) Ma, B. Q.; Gao, S.; Su, G.; Xu, G. X. *Angew. Chem., Int. Ed.* **2001**, *40*, 434.
(7) Knoeppel, D. W.; Liu, J.; Meyers, E. A.; Shore, S. G. *Inorg. Chem.*, **1998**, *37*, 4828.
(8) Du, B.; Ding, E.; Meyers, E. A.; Shore, S. G. *Inorg.Chem.* **2001**, *40*, 3637.
(9) Yan, B.; Wang, H. D.; Chen, Z. D. *Polyhedron* **2001**, *20*, 591.
(10) Yan, B.; Chen, Z.; Wang, S.; Gao, S. *Chem. Lett.* **2001**, 350.
(11) Tanase, S.; Andruh, M.; Müller, A.; Schmidtmann, M.; Mathonière, C.; Rombaut, G. *Chem. Commun.* **2001**, 1084.
(12) Kou, H. Z.; Gao, S.; Li, C. H.; Liao, D. Z.; Zhou, B. C.; Wang, R. J.; Li, Y. *Inorg. Chem.* **2002**, *41*, 4756.
(13) (a) Yan, B.; Chen, Z. *Helv. Chim. Acta* **2001**, 817. (b) Yan, B.; Chen, Z. *Trans. Met., Chem.* **2001**, *26*, 287.
(14) Liu, S.; Meyers, E. A.; Shore, S. G. *Angw. Chem., Int. Ed.* **2002**, *41*, 3609.

10.1021/ic050648i CCC: $30.25
Published on Web 08/31/2005

lanthanide ions and $[Fe(CN)_6]^{3-}$ or $[Co(CN)_6]^{3-}$: (a) $[\{Gd(DMA)_3(H_2O)_4\}_2Fe(CN)_6][Fe(CN)_6]\cdot 3H_2O$ (DMA = *N*,*N*-dimethylacetamide), an isolated trinuclear Gd−Fe−Gd complex with two approximately perpendicular cis-positioned bridging CN^- ligands between the two Gd atoms and the Fe atom.[13a] (b) $[Nd_2Fe(CN)_6(bpy)_4(H_2O)_8][Fe(CN)_6]\cdot 8H_2O$, a trinuclear Nd−Fe−Nd complex with two approximately trans-positioned bridging CN^- ligands between the two Nd atoms and the Fe atom.[19] This complex is isostructural with the complexes characterized in the present paper. We decided to synthesize and characterize this complex to study its magnetic behavior and to solve its structure in the same conditions of the other complexes of this family of trinuclear compounds.

Looking at the literature, structural changes are found when using different building blocks, different solvents, different stoichiometries, or when changing the specific lanthanide ion. Winpenny et al.,[20a] report that reactions in methanol lead to tetranuclear species with a Cu_2Ln_2 core if the ambidentate bridge 6-methyl-2-pyridonate is used and lead to tetranuclear species with a Cu_3Ln core if the ambidentate bridge 6-chloro-2-pyridonate is involved. These authors have also shown that reactions involving lanthanum nitrate and 6-chloro-2-pyridonate as bridging ligand produce different metal cores if the solvent is varied from MeOH to EtOH or MeCN.[20b] Using 6-chloro-2-pyridonate as bridged ligand, the same reaction using gadolinium, dysprosium, or erbium in place of lanthanum lead to a different product.[20c] Huang el al,[21,22] state that reactions in ethanol using the bulky ligand pivalic acid and quinoline lead to dinuclear $Co^{2+}-Ln^{3+}$ assemblies with CoTb, CoGd, and CoDy cores if the stoichiometry is Co/Ln 1:1; if the stoichiometry was Co/Ln 2:1, two trinuclear assemblies with Co_2Dy and Co_2Nd cores and a tetranuclear assembly with Co_2Er_2 core were found.

In general, using the same reactants and reaction conditions, few studies on the full lanthanide series are found. We are exploring a strategy to control the structure in the solid state that combines elements of design toward crystal engineering and the study of magnetic properties. We successfully applied this strategy in the preparation of new species starting from mononuclear species $[M(CN)_6]^{3-}$ (M = Fe^{3+}, Cr^{3+}, and Co^{3+}) as building blocks, $Ln(NO_3)_3\cdot xH_2O$, and different blocking ligands. (a) With M = Fe^{3+} or Co^{3+} and *N*,*N*′-dimethylformamide (DMF) as blocking ligand, working with the same conditions, we reported a family of 25 dinuclear complexes of formula $[Ln(DMF)_4(H_2O)_3(\mu\text{-}CN)M(CN)_5]\cdot nH_2O$ (with Ln = all lanthanide(III) ions except Pm and Lu) (Scheme 1a).[4a] Structural studies of these families show that they are isomorphous. (b) Changes in the building-block ligand modifies the structural types: using $[Cr(CN)_6]^{3-}$, $Gd(NO_3)_3\cdot 6H_2O$, DMF, and the same conditions of reaction, a one-dimensional *cis*-$[Cr(CN)_4(\mu\text{-}CN)_2Gd(H_2O)_2(DMF)_4]_n\cdot nH_2O$ was previously reported by the authors (Scheme 1b).[4c] (c) Changes in the terminal blocking ligand makes also changes in the structural types: reactions involving Ln^{3+} and $[Co(CN)_6]^{3+}$, $[Fe(CN)_6]^{3+}$, or $[Cr(CN)_6]^{3-}$ ions using bpy as terminal ligand instead of DMF lead to one-dimensional complexes of formula *trans*-$[M(CN)_4(\mu\text{-}CN)_2Ln(H_2O)(bpy)]_n\cdot XnH_2O$ (bpy = 2,2′bipyridine) with $[FeSm]_n$, $[FeGd]_n$, $[FeYb]_n$, $[CoGd]_n$, $[CoYb]_n$, and $[CrGd]_n$ cores (Scheme 1d).[4b,4c] In all the above-mentioned complexes, hydrogen bonds and $\pi-\pi$ interactions when the blocking ligand was bpy are present to give three-dimensional networks.

Scheme 1

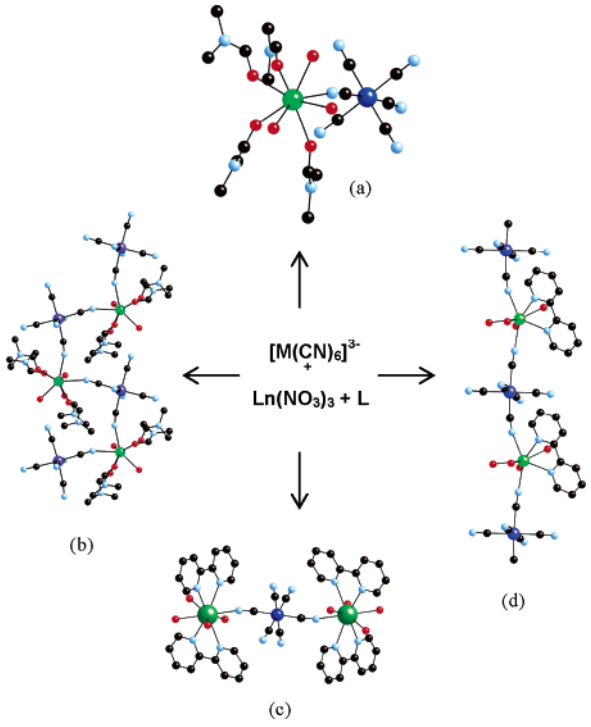

When we tried to complete this last *trans*-$[M(CN)_4(\mu\text{-}CN)_2Ln(H_2O)(bpy)]_n\cdot XnH_2O$ (M = Co^{3+}, Fe^{3+}; X = 4 or 5) series, using all lanthanide ions, new trinuclear complexes were obtained from the early lanthanides (Scheme 1c) and one-dimensional systems from the late ones. Part I of this work is, thus, focused on the characterization and the study of the magnetic behavior of the trinuclear complexes of formula: *trans*-$[Fe(CN)_4(\mu\text{-}CN)_2\{La(H_2O)_4(bpy)_2\}_2][Fe(CN)_6]\cdot 8H_2O$ (**1**), *trans*-$[Fe(CN)_4(\mu\text{-}CN)_2\{Ce(H_2O)_4(bpy)_2\}_2][Fe(CN)_6]\cdot 8H_2O$ (**2**), *trans*-$[Fe(CN)_4(\mu\text{-}CN)_2\{Pr(H_2O)_4(bpy)_2\}_2][Fe(CN)_6]\cdot 8H_2O$ (**3**), *trans*-$[Fe(CN)_4(\mu\text{-}CN)_2\{Nd(H_2O)_4(bpy)_2\}_2][Fe(CN)_6]\cdot 8H_2O$ (**4**) *trans*-$[Co(CN)_4(\mu\text{-}CN)_2\{Ce(H_2O)_4(bpy)_2\}_2]\ [Co(CN)_6]\cdot 8H_2O$ (**5**), *trans*-$[Co(CN)_4(\mu\text{-}$

(15) Kautz, J. A.; Mullica, D. F.; Cunningham, B. P.; Combs, R. A.; Farmer, J. M. *J. Mol. Struct.* **2000**, *523*, 175.
(16) Kou, H. Z.; Yang, G. M.; Liao, D. Z.; Cheng, P.; Jiang, Z. H.; Yan, S. P.; Huang, X. Y.; Wang, G. L. *J. Chem. Crystallogr.* **1998**, *28*, 303.
(17) Mullica, D. F.; Farmer, J. M.; Cunningham, B. P.; Kautz, J. A. *J. Coord. Chem.* **2000**, *49*, 239.
(18) Yan, B.; Chen, Z. *Chem. Lett.* **2000**, *11*, 1244.
(19) Yi, T.; Gao, S.; Chen, X. W.; Yan, C. H.; Li, B. G. *Acta Crystallogr.* **1998**, *C54*, 41.
(20) (a) Blake, A. J.; Gould, R. O.; Grant, C. M.; Milne, P. E.; Parson, S.; Winpenny, R. E. P. *J. Chem. Soc., Dalton Trans.* **1997**, 485 and references therein. (b) Blake, A. J.; Milne, P. E. Y. Winpenny, R. E. P. *J. Chem. Soc., Dalton Trans.* **1993**, 3727. (c) Benelli, C. Blake, A. J.; Milne, P. E. Y.; Rawson, J. M.; Winpenny, R. E. P. *Chem. Eur. J.* **1995**, *9*, 614.
(21) Cui, Y. C.; Chen, J. T.; Ren, J.; Kian, Y.; Huang, J. S. *Inorg. Chem.* **2000**, *39*, 4165.
(22) Cui, Y. C.; Chen, J. T.; Long, D. L.; Zheng, F. K.; Cheng, W. D.; Huang, J. S. *J. Chem. Soc., Dalton Trans.* **1998**, 2955.

Table 1. Crystal Parameters for **1**−**4**

	[La_2Fe](**1**)	[Ce_2Fe] (**2**)	[Pr_2Fe] (**3**)	[Nd_2Fe] (**4**)
empirical formula	$C_{52}H_{64}Fe_2La_2N_{20}O_{16}$	$C_{52}H_{64}Ce_2Fe_2N_{20}O_{16}$	$C_{52}H_{64}Fe_2N_{20}O_{16}Pr_2$	$C_{52}H_{64}Fe_2N_{20}O_{16}Nd_2$
F_w	1614.75	1617.17	1618.75	1625.41
cryst size (mm^3)	0.50 × 0.50 × 0.18	0.41 × 0.30 × 0.24	0.31 × 0.15 × 0.10	0.41 × 0.37 × 0.18
cryst habit, color	prism, yellow	prism, brown	prism, yellow	prism, yellow
crystal system	triclinic	triclinic	triclinic	triclinic
space group	$P\bar{1}$	$P\bar{1}$	$P\bar{1}$	$P\bar{1}$
Z	1	1	1	1
a (Å)	10.2122(4)	10.1999(5)	10.1882(5)	10.1849(13)
b (Å)	11.4899(4)	11.4896(5)	11.4854(6)	11.4934(14)
c (Å)	15.7032(6)	15.6600(7)	15.6703(8)	15.618(2)
α (deg)	87.195(1)	87.165(1)	87.157(1)	87.131(2)
β (deg)	87.701(1)	87.692(1)	87.596(1)	87.587(2)
γ (deg)	66.531(1)	66.409(1)	66.349(1)	66.321(2)
V ($Å^3$)	1687.69(11)	1679.38(13)	1673.53(15)	1671.7(4)
ρ (calcd) (g/cm^3)	1.588	1.599	1.606	1.615
μ_{calc} (mm^{-1})	1.738	1.830	1.932	2.030
T (K)	298(2)	298(2)	298(2)	298(2)
F(000)	810	812	814	816
transm coeff (max; min)	0.6418; 0.4770	0.6678; 0.5208	0.8303; 0.5858	0.7114; 0.4900
decay (%)	0	0	0	0.9
scan type	ϕ and ω	ϕ and ω	ϕ and ω	ϕ and ω
Θ range for data collection	1.93−28.30°	1.94−28.30°	1.94−28.28°	1.94−28.27°
total reflns	10 869	10 893	10 853	10 824
independent reflns [R(int)]	7652 [0.0133]	7659 [0.0142]	7610 [0.0210]	7604 [0.0156]
completeness to Θ_{max}	91.1%	91.6%	91.5%	91.7%
absorption correction	multiscan	multiscan	multiscan	multiscan
params refined, restraints	418, 0	418, 0	418, 0	418, 0
final R indices[a] [$I > 2\sigma(I)$]	R1 = 0.0211	R1 = 0.0232	R1 = 0.0294	R1 = 0.0231
final wR2 indices (all data)[a]	wR2 = 0.0574	wR2 = 0.0597	wR2 = 0.0678	wR2 = 0.0597
weights[b] (a, b)	0.0308, 0.6170	0.0337, 0.3665	0.0308, 0	0.0322, 0.6652
GOF on F^2	1.037	1.005	1.013	0.981
largest diff. peak and hole ($eÅ^{-3}$)	0.824 and −0.796	0.476 and −0.705	0.534 and −0.605	0.647 and −0.640

[a] $R1 = \sum||F_0| - |F_c||$ and $wR2 = \{\sum[w(F_0^2 - F_c^2)]/\sum[w(F_0^2)^2]\}^{1/2}$. [b] The weighting scheme employed was $w = [\sigma^2(F_0^2 + (aP)^2 + bP]]$ and $P = (|F_0|^2+2|F_c|^2)/3$.

$CN)_2\{Pr(H_2O)_4(bpy)_2\}_2][Co(CN)_6]\cdot 8H_2O$ (**6**), *trans*-[$Co(CN)_4(\mu$-$CN)_2\{Nd(H_2O)_4$ $(bpy)_2\}_2][Co(CN)_6]\cdot 8H_2O$ (**7**), and *trans*-[$Co(CN)_4(\mu$-$CN)_2\{Sm(H_2O)_4(bpy)_2\}_2][Co(CN)_6]\cdot 8H_2O$ (**8**). Part II of this work will be focused on the study of the magnetic behavior of the new chains obtained in the same reaction but starting from the late lanthanides, i.e., $[EuFe]_n$, $[TbFe]_n$, $[DyFe]_n$, $[HoFe]_n$, $[ErFe]_n$, $[TmFe]_n$, $[EuCo]_n$, $[TbCo]_n$, $[DyCo]_n$, $[HoCo]_n$, $[ErCo]_n$, and $[TmCo]_n$, which are isostructural between them and with those previously described by us (Scheme 1d).[4b]

Experimental Section

Materials. All starting materials were purchased from Aldrich and were used without further purification.

Synthesis of the New Complexes. *trans*-[$Fe(CN)_4(\mu$-$CN)_2\{La(H_2O)_4(bpy)_2\}_2$] $[Fe(CN)_6]\cdot 8H_2O$ (1), *trans*-[$Fe(CN)_4(\mu$-$CN)_2\{Ce(H_2O)_4(bpy)_2\}_2][Fe(CN)_6]\cdot 8H_2O$ (2), *trans*-[$Fe(CN)_4(\mu$-$CN)_2\{Pr(H_2O)_4(bpy)_2\}_2][Fe(CN)_6]\cdot 8H_2O$ (3), *trans*-[$Fe(CN)_4(\mu$-$CN)_2\{Nd(H_2O)_4(bpy)_2\}_2][Fe(CN)_6]\cdot 8H_2O$ (4). The four [$Fe^{3+}-Ln^{3+}$] complexes were obtained by adding a solution of $Ln(NO_3)_3\cdot nH_2O$ ($n = 5$ or 6) (2.2 mmol) in water (15 mL) to an equimolar solution of $K_3[Fe(CN)_6]$ in water (50 mL). To this mixture an ethanolic solution (10 mL) of 2,2′-bipyridine (3.3 mmol) was added. The solutions were left undisturbed, and well-formed orange crystals were obtained, for all of them, after several days (yields ca. 75%). Anal. Calcd for **1**, $C_{25}H_{64}Fe_2La_2N_{20}O_{16}$: C, 38.68; N, 17.35; H, 4.00. Found: C, 38.5; N, 17.3; H, 3.9. Anal. Calcd For **2**, $C_{25}H_{64}Ce_2Fe_2N_{20}O_{16}$: C, 38.62; N, 17.32; H, 3.99; Found: C, 33.7; N, 17.2; H, 3.8. Anal. Calcd For **3**, $C_{25}H_{64}Fe_2N_{20}O_{16}Pr_2$: C, 38.58; N, 17.31; H, 3.98. Found: C, 38.7; N, 17.8; H, 3.7. Anal. Calcd For **4**, $C_{25}H_{64}Fe_2N_{20}Nd_2O_{16}$: C, 38.42; N, 17.24; H, 3.97. Found: C, 38.2; N, 17.1; H 4.1.

***trans*-[$Co(CN)_4(\mu$-$CN)_2\{Ce(H_2O)_4(bpy)_2\}_2][Co(CN)_6]\cdot 8H_2O$ (5), *trans*-[$Co(CN)_4(\mu$-$CN)_2\{Pr(H_2O)_4(bpy)_2\}_2][Co(CN)_6]\cdot 8H_2O$ (6), *trans*-[$Co(CN)_4(\mu$-$CN)_2\{Nd(H_2O)_4(bpy)_2\}_2][Co(CN)_6]\cdot 8H_2O$ (7), *trans*-[$Co(CN)_4(\mu$-$CN)_2\{Sm(H_2O)_4(bpy)_2\}_2][Co(CN)_6]\cdot 8H_2O$ (8).** The four [$Co^{3+}-Ln^{3+}$] complexes were obtained by the same procedure using $K_3[Co(CN)_6]$ instead of $K_3[Fe(CN)_6]$. Well-formed colorless crystals were obtained after several days (yields ca. 70%). Anal. Calcd for **5**, $C_{25}H_{64}Ce_2Co_2N_{20}O_{16}$: C, 38.47; N, 17.26; H, 3.97. Found: C, 38.5; N, 17.1; H, 3.8. Anal. Calcd for **6**, $C_{25}H_{64}Co_2N_{20}O_{16}Pr_2$: C, 38.44; N, 17.24; H, 3.97. Found: C, 38.3; N, 17.3; H, 4.1. Anal. Calcd for **7**: $C_{25}H_{64}Co_2N_{20}Nd_2O_{16}$: C, 38.28; N, 17.17; H, 3.95. Found: C, 38.4; N, 17.1; H, 4.1.

Crystal Structure Determination: Crystal data and details on the data collection and refinement are summarized in Tables 1 and 2. The crystal data for complexes **1**−**8** were collected using a Bruker SMART CCD-based diffractometer operating at room temperature, except for complex **8**, which was recorded at 173(2) K. Intensities were collected with graphite monochromatized Mo Kα radiation ($\lambda = 0.71073$ Å) operating at 50 kV and 30 mA, using the $\omega/2\theta$ scan technique. A total of 1271 frames of intensity data were collected over a hemisphere of the reciprocal space by combination of three exposure sets. Each frame covered 0.3° in ω, and the first 50 frames were recollected at the end of data collection to monitor crystal decay (Tables 1 and 2). The refinement method employed was full-matrix least-squares on F^2. The results of the integration process are summarized in Tables 1 and 2. Absorption corrections were applied using the SADABS program[23] (the maximum and minimum transmission coefficients are in Tables 1 and 2). The structures were solved using the Bruker SHELXTL-PC software[24]

Table 2. Crystal Parameters for **5**−**8**

	[Ce_2Co] (**5**)	[Nd_2Co] (**6**)	[Pr_2Co] (**7**)	[Sm_2Co] (**8**)
empirical formula	$C_{52}H_{64}Ce_2Co_2N_{20}O_{16}$	$C_{52}H_{64}Co_2Nd_2N_{20}O_{16}$	$C_{52}H_{64}Co_2N_{20}O_{16}Pr_2$	$C_{52}H_{64}Co_2N_{20}O_{16}Sm_2$
F_w	1623.33	1631.75	1624.91	1643.79
cryst size (mm^3)	0.33 × 0.24 × 0.19	0.46 × 0.25 × 0.11	0.50 × 0.46 × 0.30	0.45 × 0.35 × 0.20
cryst habit, color	prism, colorless	prism, colorless	prism, yellow	prism, colorless
crystal system	triclinic	triclinic	triclinic	triclinic
space group	$P\bar{1}$	$P\bar{1}$	$P\bar{1}$	$P\bar{1}$
Z	1	1	1	1
a (Å)	10.2305(5)	10.1529(18)	10.1612(13)	10.0952(5)
b (Å)	11.5190(6)	11.443(2)	11.4376(15)	11.3897(6)
c (Å)	15.6614(7)	15.481(3)	15.524(2)	15.4801(8)
α (deg)	87.009(1)	86.955(3)	86.931(2)	86.997(1)
β (deg)	87.742(1)	87.608(3)	87.685(2)	87.380(1)
γ (deg)	66.525(1)	66.418(3)	66.436(2)	66.456(1)
V ($Å^3$)	1690.21(14)	1645.6(5)	1651.0(4)	1628.91(14)
ρ (calcd) (g/cm^3)	1.595	1.646	1.634	1.676
μ_{calc} (mm^{-1})	1.880	2.125	2.021	2.356
T (K)	298(2)	298(2)	298(2)	173(2)
F(000)	814	818	816	822
transm coeff (max; min)	0.7165; 0.5759	0.7999; 0.4415	0.5823; 0.4314	0.6502; 0.4170
decay (%)	0	0	0	0.4
scan type	ϕ and ω	ϕ and ω	ϕ and ω	ϕ and ω
Θ range for data collection	1.30−28.30°	1.94−28.36°	2.19−28.34°	1.32−26.37°
total reflns	10 855	10 695	10 697	10 148
independent reflns [R(int)]	7625 [0.0168]	7516 [0.0228]	7521 [0.0130]	6604 [0.0270]
completeness to Θ_{max}	90.5%	91.3%	91.3%	99%
absorption correction	multiscan	multiscan	multiscan	multiscan
params refined, restraints	419, 0	419, 0	419, 0	418, 0
final R indices[a] [$I > 2\sigma(I)$]	R1 = 0.0236	R1 = 0.0274	R1 = 0.0196	R1 = 0.0294
final wR2 indices (all data)[a]	wR2 = 0.0577	wR2 = 0.0758	wR2 = 0.0506	wR2 = 0.0768
weights[b] (a, b)	0.0258, 0.3741	0.0488, 0.1596	0.0230, 0.5808	0.0539, 0
GOF on F^2	1.033	0.966	1.054	1.001
largest diff. peak and hole ($eÅ^{-3}$)	0.380 and −0.521	1.011 and −1.135	0.465 and −0.396	1.756 and −1.618

[a] $R1 = \sum||F_0| - |F_c||$ and $wR2 = \{\sum[w(F_0^2 - F_c^2)]/\sum[w(F_0^2)^2]\}^{1/2}$. [b] The weighting scheme employed was $w = [\sigma^2(F_0^2 + (aP)^2 + bP]]$ and $P = (|F_0|^2+2|F_c|^2)/3$.

by direct methods and refined by full-matrix least-squares methods on F^2. All non-hydrogen atoms were refined anisotropically. Hydrogen atoms were included in calculated positions and refined in the riding mode, except those of water molecules that were located on residual density maps, but then fixed their positions and refined in the riding mode.

Physical Measurements. Magnetic measurements were carried out in the "Servei de Magnetoquímica (Universitat de Barcelona)" on polycrystalline samples (20 mg) with a Quantum Design SQUID MPMS-XL magnetometer working in the 2−300 K range. The magnetic field was 0.1 T. The field-dependent magnetization was measured at 2 K in the applied magnetic field range 0−5 T. The diamagnetic corrections were evaluated from Pascal's constants.

Results and Discussion

Description of the Structures of *trans*-[Fe(CN)$_4$(μ-CN)$_2$-{La(H$_2$O)$_4$(bpy)$_2$}$_2$][Fe(CN)$_6$]·8H$_2$O (1), *trans*-[Fe(CN)$_4$-(μ-CN)$_2${Ce(H$_2$O)$_4$(bpy)$_2$}$_2$][Fe(CN)$_6$]·8H$_2$O (2), *trans*-[Fe(CN)$_4$(μ-CN)$_2${Pr(H$_2$O)$_4$(bpy)$_2$}$_2$][Fe(CN)$_6$]·8H$_2$O (3), *trans*-[Fe(CN)$_4$(μ-CN)$_2${Nd(H$_2$O)$_4$(bpy)$_2$}$_2$][Fe(CN)$_6$]·8H$_2$O (4), *trans*-[Co(CN)$_4$(μ-CN)$_2${Ce(H$_2$O)$_4$ (bpy)$_2$}$_2$][Co(CN)$_6$]·8H$_2$O (5), *trans*-[Co(CN)$_4$(μ-CN)$_2${Pr(H$_2$O)$_4$(bpy)$_2$}$_2$]-[Co(CN)$_6$]·8H$_2$O (6), *trans*-[Co(CN)$_4$(μ-CN)$_2${Nd(H$_2$O)$_4$-(bpy)$_2$}$_2$][Co(CN)$_6$]·8H$_2$O (7), and *trans*-[Co(CN)$_4$(μ-CN)$_2$-{Sm(H$_2$O)$_4$(bpy)$_2$}$_2$][Co(CN)$_6$]·8H$_2$O (8). The structure of these complexes was determined by X-ray crystallography.

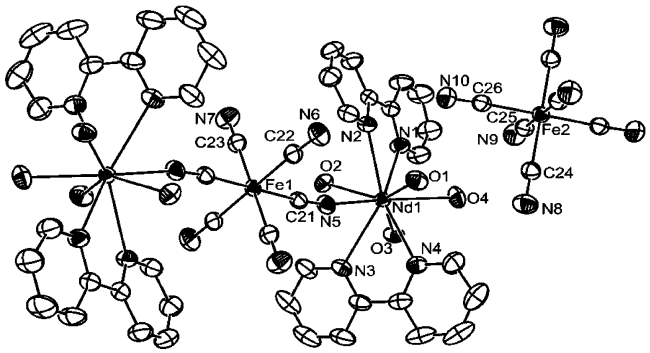

Figure 1. ORTEP view of complex *trans*-[Fe(CN)$_4$(μ-CN)$_2${Nd(H$_2$O)$_4$-(bpy)$_2$}$_2$][Fe(CN)$_6$]·8H$_2$O (**4**) with atom labeling scheme. Complexes **1**, **2**, **3**, **5**, **6**, **7**, and **8** show a similar structure (they are isostructural).

In all eight cases, the crystal system is triclinic with space group $P\bar{1}$. Their crystallographic analysis revealed that they all are isomorphous (Tables 1 and 2). Their structure is built by trinuclear cations, $[M(CN)_4(\mu\text{-}CN)_2\{Ln(H_2O)_4(bpy)_2\}_2]^{3+}$, $[M(CN)_6]^{3-}$, and solvent water molecules. As an example, an ORTEP view of the [Nd_2Fe] (**4**) complex with the atom-labeling scheme is given in Figure 1. Selected distances and angles are given in Tables 3 and 4 for the [Ln_2Fe] and [Ln_2Co] complexes, respectively. The structure of the centrosymmetric trinuclear cation consists of a cyano-bridged array of $M(CN)_6$ (M = Fe^{3+} or Co^{3+}) and two $Ln(H_2O)_4$-$(bpy)_2$ fragments, the M1 atom is connected to two Ln atoms

(23) Sheldrick, G. M. *SADABS, A Program for Empirical Absorption Correction of Area Detector Data*; University of Göttingen: Göttingen, Germany, 1996. Based on the method of Robert Blessing: Blessing, R. H. *Acta Crystallogr.* **1995**, *A51*, 33.

(24) Sheldrick, G. M. *SHELXS-97, A Program for Solving Crystal Structures and Crystal Structure Refinement*; University of Göttingen: Göttingen, Germany, 1997.

Table 3. Selected Bond Lengths (Å) and Angles (deg) for **1**−**4**

	[La_2Fe] (**1**)	[Ce_2Fe] (**2**)	[Pr_2Fe] (**3**)	[Nd_2Fe] (**4**)
Ln(1)−O(1)	2.490(2)	2.505(2)	2.449(2)	2.475(2)
Ln(1)−O(2)	2.531(2)	2.468(2)	2.491(2)	2.432(2)
Ln(1)−O(3)	2.592(2)	2.527(2)	2.551(2)	2.492(2)
Ln(1)−O(4)	2.550(2)	2.568(2)	2.511(2)	2.537(2)
Ln(1)−N(1)	2.748(2)	2.727(2)	2.711(2)	2.705(2)
Ln(1)−N(2)	2.755(2)	2.733(2)	2.718(2)	2.702(2)
Ln(1)−N(3)	2.757(2)	2.737(2)	2.720(2)	2.717(2)
Ln(1)−N(4)	2.694(2)	2.672(2)	2.653(2)	2.641(2)
Ln(1)−N(5)	2.613(2)	2.589(2)	2.569(2)	2.552(2)
Fe(1)−C(21)	1.937(2)	1.933(2)	1.937(3)	1.939(2)
Fe(1)−C(22)	1.947(2)	1.927(2)	1.951(3)	1.932(2)
Fe(1)−C(23)	1.929(2)	1.947(2)	1.929(3)	1.954(2)
Fe(2)−C(24)	1.929(2)	1.942(2)	1.924(3)	1.945(3)
Fe(2)−C(25)	1.941(2)	1.947(2)	1.945(3)	1.951(3)
Fe(2)−C(26)	1.942(2)	1.931(2)	1.931(3)	1.933(3)
N(5)−C(21)	1.149(3)	1.148(3)	1.149(4)	1.148(3)
Ln(1)−N(5)−C(21)	167.5(2)	167.7(2)	168.0(2)	168.6(2)
Fe(1)−C(21)−N(5)	174.8(2)	174.9(2)	174.6(3)	174.5(2)

Table 4. Selected Bond Lengths (Å) and Angles (deg) for **5**−**8**

	[Ce_2Co] (**5**)	[Pr_2Co] (**6**)	[Nd_2Co] (**7**)	[Sm_2Co] (**8**)
Ln(1)−O(1)	2.523(2)	2.4415(15)	2.428(2)	2.449(2)
Ln(1)−O(2)	2.477(2)	2.4480(15)	2.471(2)	2.402(2)
Ln(1)−O(3)	2.546(2)	2.5464(15)	2.531(2)	2.457(2)
Ln(1)−O(4)	2.582(2)	2.5086(14)	2.491(2)	2.502(2)
Ln(1)−N(1)	2.743(2)	2.7099(17)	2.636(2)	2.617(2)
Ln(1)−N(2)	2.744(2)	2.7081(16)	2.709(2)	2.692(2)
Ln(1)−N(3)	2.756(2)	2.7188(17)	2.700(2)	2.673(2)
Ln(1)−N(4)	2.685(2)	2.6466(18)	2.697(2)	2.687(2)
Ln(1)−N(5)	2.610(2)	2.5700(17)	2.547(2)	2.535(3)
Co(1)−C(21)	1.904(2)	1.8932(19)	1.891(3)	1.902(3)
Co (1)−C(22)	1.914(2)	1.880(2)	1.881(3)	1.887(3)
Co(1)−C(23)	1.894(2)	1.903(2)	1.904(3)	1.911(3)
Co(2)−C(24)	1.907(2)	1.898(2)	1.893(3)	1.903(4)
Co(2)−C(25)	1.909(2)	1.896(2)	1.908(3)	1.893(3)
Co (2)−C(26)	1.901(2)	1.887(2)	1.890(3)	1.903(3)
N(5)−C(21)	1.148(3)	1.141(3)	1.152(4)	1.146(4)
Ln(1)−N(5)−C(21)	167.9(2)	168.15(17)	168.4(2)	168.7(3)
Co(1)−C(21)−N(5)	174.8(2)	174.81(18)	174.8(2)	174.3(3)

through two trans bridged cyano groups. The Ln^{3+} atom is nine-coordinated. Five nitrogen atoms surround the Ln^{3+} ion: four of the two bpy ligands and one of the bridging CN^- ligand. Four oxygen atoms of water molecules complete their coordination. The Ln−O distances range from 2.60 to 2.40 Å and the Ln−N range from 2.76 to 2.53 Å; the shortest distances correspond to the nitrogen atom of the CN^- bridge. In the trinuclear cation, six CN^- ligands surround the M^{3+} (Fe1, Co1) ion, which lies on a center of symmetry, in a distorted octahedral environment. The Fe−C distances range from 1.95 to 1.92 Å and the Co−C distances range from 1.91 to 1.88 Å. The $[M(CN)_6]^{3-}$ ($M = Fe^{3+}$, Co^{3+}) counteranion is octahedral with M^{3+} lying on a center of symmetry. The lowest M−C distances correspond as expected to the $[Co(CN)_6]^{3-}$ ion. The Ln−M (M = Fe, Co) intramolecular distances are 5.684 Å for **1**, 5.621 Å for **2**, 5.608 Å for **3**, 5.594 Å for **4**, 5.614 Å for **5**, 5.546 Å for **6**, 5.558 Å for **7**, and 5.538 Å for **8**. The Ln−M−Ln angles are 179.98° for **1**, 180.00° for **2**, 179.98° for **3**, 180.00° for **4**, 180.00° for **5**, 180.00° for **6**, 180.00° for **7**, and 179.97° for **8**, indicating the trans configuration imposed by the inversion center at the transition metal atom.

Their supramolecular structures are created by hydrogen bonding and $\pi-\pi$ stacking interactions. The trinuclear cations are self-assembled through hydrogen bonds in very different pathways due to the high number of atoms that could participate into them. The O1S, O2S, O3S, and O4S atoms of the water molecules of crystallization participate in the supramolecular structure, the O1, O2, O3, and O4 oxygen atoms of the coordinated water molecules to the lanthanide ion and the six nitrogen atoms (N8−N10) of the $[M(CN)_6]^{3-}$ counteranion, giving an extensive 3D network. Hydrogen bond distances and angles are shown for complexes **1**−**8** (Supporting Information, Tables S1 and S2). As an example of these eight isomorphous complexes, in Figure 2 the different ways and the atoms involved in the three-dimensional trinuclear self-assembled structure through hydrogen bonds for complex [Nd_2Co] (**7**) are shown. Figure 2a and b shows the chains built through the oxygen O1S and O2S atoms from water molecules of crystallization: these chains could be described as an alternation of trinuclear cations $[Ln^{3+}-M^{3+}-Ln^{3+}]^{3+}$ and $[M(CN)_6]^{3-}$counteranions linked through water molecules. Figure 2c shows the chain built though the O3S atom from another water molecule, with the trinuclear units $[Ln^{3+}-M^{3+}-Ln^{3+}]^{3+}$ self-assembled in pairs through the O3S atom giving an hexanuclear system, and the hexanuclear units are linked between them through the $[M(CN)_6]^{3-}$ counteranion. Figure 2d shows the intra-trinuclear hydrogen bonds through the O(4S) atom. Figure 2e and f shows direct interaction between the trinuclear entities and the counteranion giving a chain and a two-dimensional network, respectively, in which water molecules coordinated to the lanthanide ion and nitrogen atoms of the $[Fe(CN)_6]^{3-}$ counteranion participate. Some of these six self-assemblies (a−f) are interconnected between them to give a complicated 3D network of hydrogen bonds. An additional hydrogen bond between O(3S) and O(4S) must be taken into account and the atoms that in Figure 2 appear with (*) are common in some of these pathways. The pathways shown in Figure 2a and b are linked between them through O1S and O4S; the pathways shown in Figure 2a and c have in common the nitrogen atoms N7 and N8; the pathways shown in Figure 2a and b have in common the oxygen atom O1; the pathways shown in Figure 2d and e have in common the oxygen atom O2. As shown in Figure 3, for the [Nd_2Co] complex as example, the bpy ligands of neighboring trinuclear entities exhibit weak $\pi-\pi$ interactions, providing additional stabilization of the crystal structure. Intermolecular stacking distances between centroids of the bpy rings are shown for all complexes in Table 5.

Shape Measure. The analysis of the nine-vertex coordination polyhedra of the lanthanide cations in these complexes is made easier and more accurate with the help of the continuous shape measures (CShM) proposed by Avnir et al.[25,26] These measures provide a way of quantitatively evaluating the loss of shape or symmetry, so as to estimate the degree of distortion of a particular coordination polyhedron from some chosen ideal polyhedron. Stereochemical

(25) Avnir, D.; Katzenelson, O.; Keinan, S.; Pinsky, M.; Pinto, M.; Salomon, Y.; Zabrodsky Hel-Or, H. In *Concepts in Chemistry: A Contemporary Challenge*; Rouvray, D. H., Ed.; Research Studies Press Ltd.: Tauton, England, 1996.
(26) Zabrodsky, H.; Peleg, S.; Avnir, D. *J. Am Chem. Soc*. **1992**, *114*, 7843.

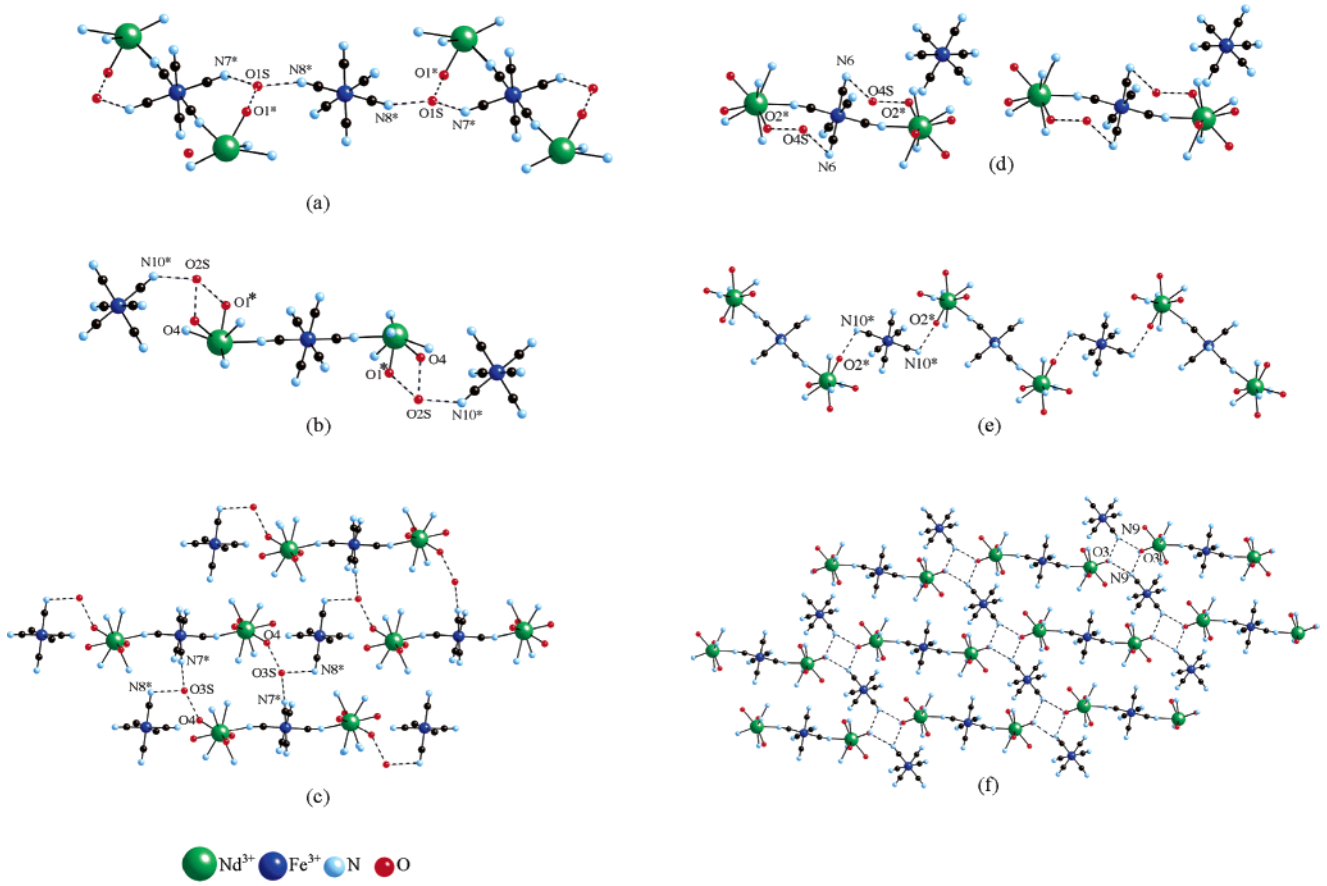

Figure 2. Schematic representation, for complex *trans*-$[Co(CN)_4(\mu\text{-}CN)_2\{Nd(H_2O)_4(bpy)_2\}_2][Co(CN)_6]\cdot 8H_2O$ (**7**), of different pathways in which the trinuclear cations are self-assembled through hydrogen bonds. Complexes **1**, **2**, **3**, **4**, **5**, **6**, and **8** show similar self-assembly.

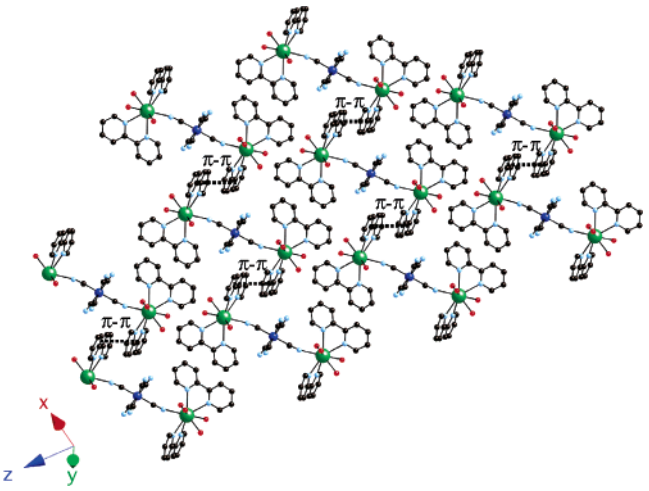

Figure 3. Schematic representation of the $\pi-\pi$ interactions of *trans*-$[Co(CN)_4(\mu\text{-}CN)_2\{Nd(H_2O)_4(bpy)_2\}_2][Co(CN)_6]\cdot 8H_2O$ (**7**). Complexes **1**, **2**, **3**, **4**, **5**, **6**, and **8** show similar $\pi-\pi$ interactions.

studies of polyhedral structures having between four and eight vertexes on the basis of CShM have been published by Alvarez et al.[27] The same authors have published a report about minimal distortion pathways in polyhedral rearrangements that allows for an easy identification of structures that lie along the interconversion pathways between two ideal polyhedra.[28]

The calculation of continuous shape measure of the coordination sphere of a given atom (polyhedron Q), relative to an ideal polyhedron, *P*, requires the knowledge of the *N* vectors $\vec{q}_i$ describing the 3*N* Cartesian coordinates q_K, as well as the corresponding vectors containing the coordinates p_K of the ideal polyhedron. The ideal shape is then rotated, translated, and scaled in such a way as to minimize the distance function in eq 1, which then gives the shape measure of the investigated structure, *Q*, relative to the ideal shape P, $S_Q(P)$. In eq 1, $\vec{q}_0$ is the position vector of the geometric center of *Q*.[28]

$$S_Q(P) = \min\left[\frac{\sum_{i=1}^{N}|\vec{q}_i - \vec{p}_i|}{\sum_{i=1}^{N}|\vec{q}_i - \vec{q}_0|}\right] \times 100 \qquad (1)$$

Table 5. Distances between bpy Ring Centroids (Å)[a]

	$[La_2Fe]$(**1**)	$[Ce_2Fe]$(**2**)	$[Pr_2Fe]$(**3**)	$[Nd_2-Fe]$(**4**)
Cg(1)−Cg(2)	3.750	3.756	3.759	3.765
	$[Ce_2Co]$(**5**)	$[Nd_2Co]$(**6**)	$[Pr_2Co]$(**7**)	$[Sm_2Co]$(**8**)
Cg(1)−Cg(2)	3.750	3.737	3.734	3.717

[a] Cg(1) ring of N3; Cg(2) ring of N4.

(27) Alvarez, S.; Alemany, P.; Casanova, D.; Cirera, J.; Llunell, M.; Avnir, D. *Coord. Chem. Rev.*, in press
(28) Casanova, D.; Cirera, J., Llunell, M.; Alemany, P.; Avnir, D.; Alvarez, S. *J. Am. Chem. Soc.* **2004**, *126*, 1755.

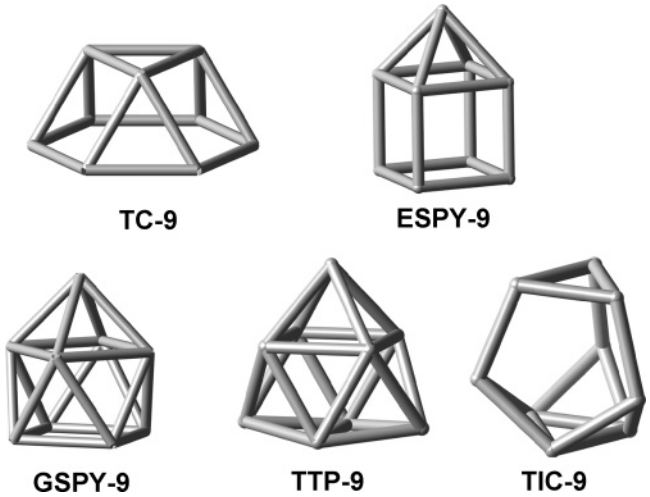

Figure 4. Ideal nine-vertex Johnson polyhedra: TC = triangular cupola; ESPY = elongated square pyramid; GSPY = gyroelongated square pyramid; TTP = triaugmented trigonal prism; and TIC = tridiminished icosahedron.

$S_Q(P) = 0$ corresponds to a structure, Q, fully coincident in shape with the reference polyhedron, P, whereas the maximum allowed value is $S_Q(P) = 100$, which corresponds to the hypothetical case in which all atoms of Q occupy the same point in the space.

To carry out a CShM-based assignment of the coordination polyhedra (nine coordination) of the lanthanide ions that constitute the object of Part I of this work, we had to establish first the reference polyhedra. As ideal shapes we have considered the planar enneagon (EP-9), the octogonal pyramid (OPY-9) and the heptagonal bipyramid (HBPY-9), together with the five nine-vertex Johnson polyhedra[29a] employed by Kepert[29b] and shown in a schematic way in Figure 4. These are the triangular cupola (TC-9), the elongated square pyramid (ESPY-9, also called capped cube), the gyroelongated square pyramid (GSPY-9, also known as capped square antiprism), the triaugmented (or tricapped) trigonal prism (TTP-9), and the tridiminished icosahedron (TIC-9). The Johnson polyhedra have, by definition, regular polygons as faces and, in most cases, quite different distances from the center to the capping vertexes, as compared to those to the others vertexes of the polyhedron. Although such polyhedra are useful for the stereochemical description of metal clusters, in which the edge lengths (bond lengths) are all similar, they are not appropriate for coordination polyhedra, in which it is the center-to-vertex distances that are all nearly equivalent.[27] Therefore, we have employed for some polyhedra two alternative reference shapes, a Johnson polyhedron (labeled as, e.g., J-GSPY) and its spherical counterpart (labeled as, e.g., s-GSPY) corresponding to a hard spheres model.

The results of the CShMs for the lanthanides in the compounds reported here give high values (i.e., larger than 17.2 in all cases) for the enneagon, the octogonal pyramid, and the heptagonal bipyramid, which can therefore be ruled out for the description of their coordination spheres. The CShM results relative to other polyhedra are presented in Table 6. From those results, we can conclude that our coordination polyhedra are closest to the spherical version of the gyroelongated square pyramid polyhedron (s-GSPY-9), although the corresponding measures relative to the triagumented trigonal prism (s-TTP-9) are not much larger and the stereochemical assignment deserves a closer look. First, we must consider that the experimental structures might be along the interconversion path between s-GSPY-9 and s-TTP-9, a possibility that can be evaluated by means of the path deviation function.[28] In short, a deviation of, e.g., 0.10 means that the distance of the analyzed structure to the path is a 10% of the length of the path. The values of the deviation function found for the eight compounds are all larger than 0.67, clearly indicating that they cannot be considered as intermediate between those two ideal polyhedra. We can then admit that the deviations from an ideal polyhedron (CShM values in the ranges 1.37−1.44 for s-GSPY-9 and 1.61−1.79 for s-TTP-9) are in part attributable to our specific choice of the reference shapes (the hard spheres model) and that an alternative choice with the same symmetry (C_{4v} and D_{3h}, respectively) could better represent the experimental coordination spheres. We have therefore decided to analyze the C_4 and C_3 symmetry contents of those coordination polyhedra, to see if these can discriminate between the two possible descriptions. The results, given as $S(C_4)$ and $S(C_3)$ in Table 6, clearly indicate that the lanthanide environments are much better described as having a C_4 than a C_3 symmetry axis, thus confirming that the best stereochemical description corresponds to a gyroelongated square pyramid. Furthermore, the deviations from the reference GSPY-9 and from C_4 symmetry show a nice linear correlation, indicating that loss of C_4 symmetry produced by inequivalence in bond distances and by the bite angles of the bpy ligands account for a good part of the deviation from that polyhedron.

Once it is clear that the lanthanide coordination spheres correspond to GSPY-9, it is straightforward to complete the stereochemical description by recognizing that the apical position of such a polyhedron is occupied in all cases by an N atom of a bpy ligand; the two bidentate ligands are always in the relative positions schematically shown in **A**, where the bold lines represent the chelating ligands. It is to be noted that the Ln−N bonds to the bpy ligands are of two different types: the apical and the two basal N atoms have practically the same bond distance (with an esd of, at most, 0.010 Å in each compound), whereas the bond distance to N′ is systematically shorter by 0.064(3) Å. Another interesting feature of the conformation shown in **A** is that it is chiral. Since each lanthanide is related to the other one by the inversion center at the transition metal atom that is bridging them, there are two enantiomeric coordination spheres in an achiral trinuclear unit (**B**).

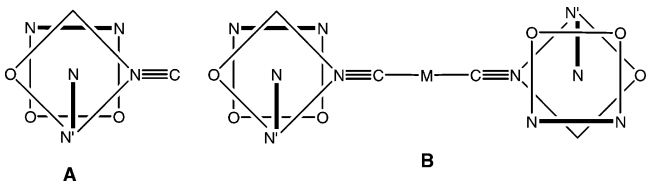

(29) (a) Alvarez, S. *Dalton Trans.* **2005**, 2209. (b) Kepert, D. L. *Inorganic Stereochemistry*; Springer: Heidelbert, 1982.

Table 6. Continuous Shape and Symmetry Measures of the Coordination Polyhedra of the Lanthanides[a]

structure	J-TC-9	J-ESPY-9	J-GSPY-9	s-GSPY-9	J-TTP-9	s-TTP-9	J-TIC-9	C_4	C_3
[La_2Fe] (**1**)	16.57	10.22	1.55	1.43	3.14	1.79	13.72	0.79	2.16
[Ce_2Fe] (**2**)	16.58	10.24	1.51	1.41	3.09	1.74	13.65	0.76	2.14
[Pr_2Fe] (**3**)	16.63	10.30	1.47	1.38	3.02	1.69	13.61	0.73	2.13
[Nd_2Fe] (**4**)	16.61	10.28	1.44	1.38	2.97	1.69	13.55	0.72	1.26
[Ce_2Co] (**5**)	16.65	10.22	1.52	1.42	3.07	1.42	13.54	0.76	1.31
[Pr_2Co] (**6**)	16.64	10.24	1.47	1.38	3.01	1.70	13.52	0.73	2.14
[Nd_2Co] (**7**)	16.62	10.29	1.45	1.37	2.99	1.68	13.48	0.72	1.25
[Sm_2Co] (**8**)	16.69	10.17	1.43	1.39	2.88	1.62	13.36	0.73	1.17

[a] See Figure 4 for labeling of ideal polyhedra.

Magnetic Studies. Magnetic measurements were performed for the eight [Ln_2Fe] and [Ln_2Co] complexes. The Ln^{3+} and the Fe^{3+} ions possess a first-order angular momentum, which prevents the use of a spin-only Hamiltonian for isotropic exchange. Not much is known about the nature of the exchange interaction of rare earth ions between themselves and with other magnetic groups because the large orbital contribution of these ions makes a quantitative interpretation of the magnetic data of their complexes very complicated. Furthermore, due to the inner nature of the 4f orbitals with respect to the 3d ones, these ions are usually involved in weak exchange coupling interactions, whose magnitude is comparable with that arising from the crystal field splitting of the ground *J* multiplet of the ion. The difficulty in having quantitative information on both these contributions has so far reduced the analysis of the magnetic properties of the anisotropic lanthanides mainly at a qualitative level, especially in molecular complexes. The most diffuse experimental approach to separate the different contributions of crystal field and exchange coupling to the magnetic properties in either heterometallic or lanthanide-radical complexes involves the determination of magnetic properties of a corresponding complex in which the second spin carrier is substituted by a diamagnetic analogue, giving rise to comparable ligand field effects on the lanthanides.[30,4a,4b] Together with the [Ln_2Fe] complexes, we attempted to synthesize and characterize the homologous [Ln_2Co] and [La_2Fe] complexes to use the typical empirical approach, mentioned above, to obtain insights into the nature of the [Ln_2Fe] coupling. The approach consists of comparing their magnetic susceptibility data with the corresponding isostructural [Ln_2Co] compounds together with the magnetic properties of the [La_2Fe] complex to take the anisotropy of the Fe^{3+} ion into account. The Co^{3+} and the La^{3+} ions are obviously diamagnetic, and the deviation of the magnetic susceptibility of these compounds with respect to the Curie law is due entirely to the thermal population of the Ln^{3+} Stark components and the anisotropy of Fe^{3+}, respectively. The comparison of the experimental magnetization at low temperature of the exchange coupled system with that of the corresponding uncorrelated spin systems constitutes a further way to discriminate the sign of the coupling. More explicitly, the experimental magnetization of every [Ln_2Fe] compound is compared with the sum of the [Ln_2Co] and [La_2Fe] magnetization curves, that is, the uncorrelated spin systems. Indeed if the *M* vs *H* curve of the coupled system is running below the curve of the noncorrelated system, an antiferromagnetic interaction within the molecular spin system is revealed, while the reverse would be true for a ferromagnetic situation.[31]

For most of the rare-earth compounds, the $\chi_M T$ value at room temperature is close to what is predicted in the free-ion approximation for the cases where only one level, $^{2S+1}L_j$, is thermally populated and second-order contributions are ignored.[32] For the complexes containing the Sm^{3+} ion, the magnetic susceptibility is affected by the thermally populated excited states because of the spin−orbit coupling.

***trans*-[Fe(CN)$_4$(μ-CN)$_2${Ce(H$_2$O)$_4$(bpy)$_2$}$_2$][Fe(CN)$_6$]·8H$_2$O (2) and *trans*-[Co(CN)$_4$(μ-CN)$_2${Ce(H$_2$O)$_4$(bpy)$_2$}$_2$]-[Co(CN)$_6$]·8H$_2$O (5).** The temperature dependence of $\chi_M T$

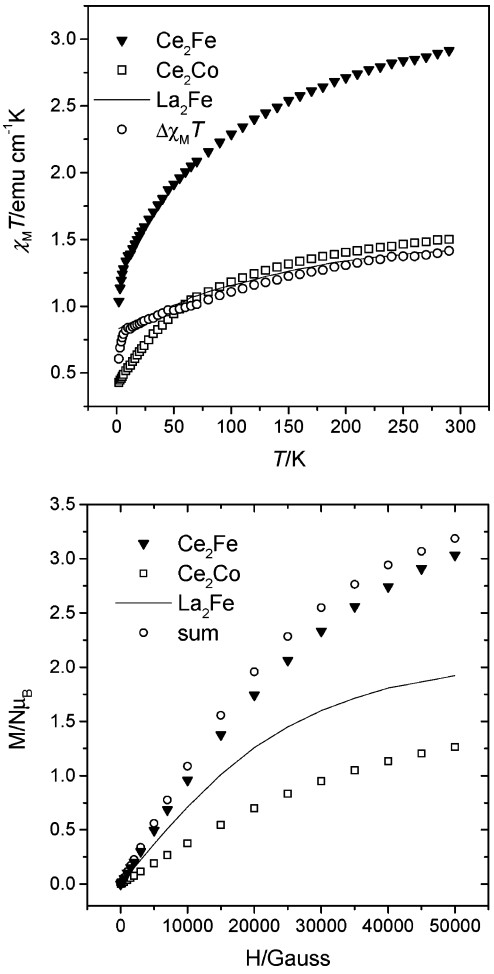

Figure 5. Top: Thermal dependence at 0.1 T of $\chi_M^{[Ce_2Fe]}T$, $\chi_M^{[Ce_2Co]}T$, $\chi_M^{[La_2Fe]}T$, and $\Delta\chi_M T = \chi_M^{[Ce_2Fe]}T - \chi_M^{[Ce_2Co]}T$. Bottom: magnetization vs *H* (2 K) of $M^{[Ce_2Fe]}$, $M^{[Ce_2Co]}$, $M^{[La_2Fe]}$, and sum = $M^{[Ce_2Fe]} + M^{[Ce_2Co]}$.

(30) (a) Costes, J. P.; Dahan, F.; Dupuis, A.; Laurent, J. P. *Chem. Eur. J.* **1998**, *9*, 1616. (b) Caneschi, A.; Dei, A.; Gatteschi, D.; Poussereau, S.; Sorace, L. *Dalton Trans.* **2004**, 1048 and references therein.

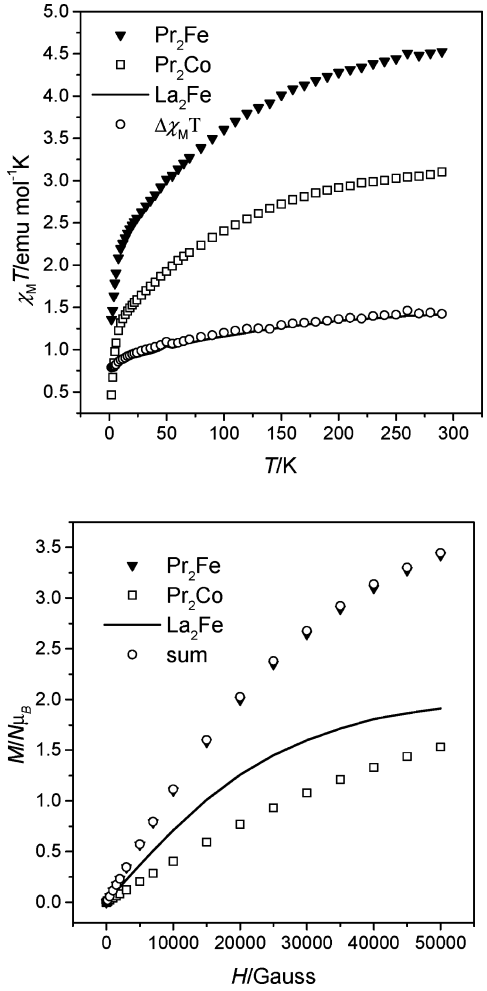

Figure 6. Thermal dependence at 0.1 T of $\chi_M^{[Pr_2Fe]}T$, $\chi_M^{[Pr_2Co]}T$, $\chi_M^{[La_2Fe]}T$ and $\Delta\chi_M T = \chi_M^{[Pr_2Fe]}T - \chi_M^{[Pr_2Co]}T$. Bottom: magnetization vs H (2 K) of $M^{[Pr_2Fe]}$, $M^{[Pr_2Co]}$, $M^{[La_2Fe]}$, and sum $= M^{[Pr_2Fe]} + M^{[Pr_2Co]}$.

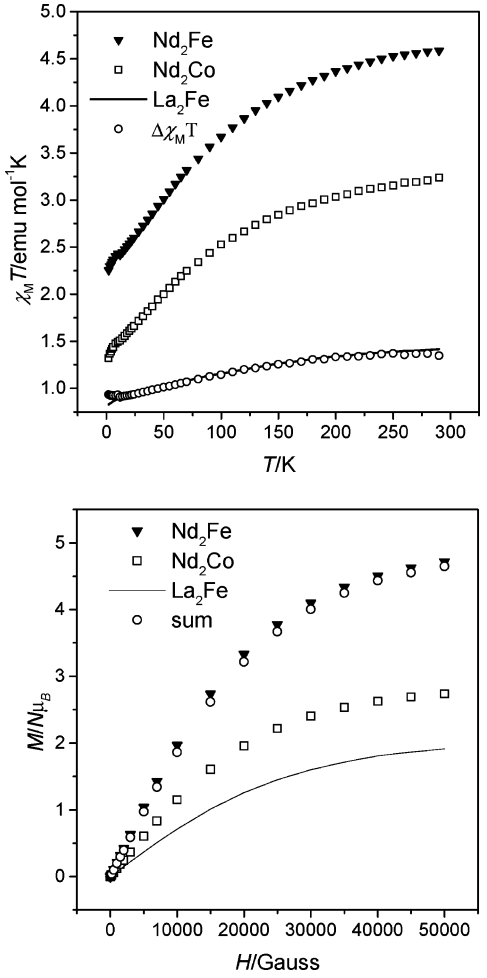

Figure 7. Thermal dependence at 0.1 T of $\chi_M^{[Nd_2Fe]}T$, $\chi_M^{[Nd_2Co]}T$, $\chi_M^{[La_2Fe]}T$ and $\Delta\chi_M T = \chi_M^{[Nd_2Fe]}T - \chi_M^{[Nd_2Co]}T$. Bottom: magnetization vs H (2 K) of $M^{[Nd_2Fe]}$, $M^{[Nd_2Co]}$, $M^{[La_2Fe]}$, and sum $= M^{[Nd_2Fe]} + M^{[Nd_2Co]}$.

for complex [Ce_2Co] is shown at the top of Figure 5. At 290 K, the $\chi_M T$ value is approximately equal to 1.50 cm^3 mol^{-1} K, close to the expected value, in the free-ion approximation, for two isolated Ce^{3+} ($^2F_{5/2}$) ions (1.6 cm^3 mol^{-1} K) and decreases with temperature to 0.43 cm^3 mol^{-1} K. The temperature dependence of $\chi_M T$ for the [Ce_2Fe] complex is also shown at the top of Figure 5. At 290 K, the$\chi_M T$ value is approximately equal to 2.91 cm^3 mol^{-1} K, while it decreases with temperature to 1.04 cm^3 mol^{-1} K. To understand the importance of the anisotropy of $Fe^{3+}{}_{LS}$, the susceptibility data ($\chi_M T$) of [La_2Fe] are also shown in the same figure. The $\Delta\chi_M T$ vs T curve is superimposable with the $\chi_M T$ vs T curve of the [La_2Fe] complex until approximately 8 K, indicating that no exchange interaction is active down to this temperature. From 8 K, $\Delta\chi_M T$ decreases with regard to the $\chi_M T$ curve of [La_2Fe]. At these low temperatures, intertrimer interactions take place due to the strong hydrogen bonds present in the structure, so the decrease in $\Delta\chi_M T$ at very low temperature could be due to the fact that the hydrogen bonds present in [Ce_2Fe] complex are stronger than those present in [Ce_2Co] complex and/or a very weak antiferromagnetic interaction between the Ce^{3+} and Fe^{3+} ions.

The experimental magnetization of [Ce_2Fe] at 2 K (Figure 5 bottom) shows a small deviation at high fields, being lower than that of the uncorrelated spin system, corroborating a very weak antiferromagnetic coupling

***trans*-[Fe(CN)$_4$(μ-CN)$_2${Pr(H$_2$O)$_4$(bpy)$_2$}$_2$][Fe(CN)$_6$]·8H$_2$O (3) and *trans*-[Co(CN)$_4$ (μ-CN)$_2${Pr(H$_2$O)$_4$(bpy)$_2$}$_2$]-[Co(CN)$_6$]·8H$_2$O (6).** The temperature dependence of $\chi_M T$ for complex [Pr_2Co] is shown at the top of Figure 6. At 290 K, the $\chi_M T$ value is approximately equal to 3.10 cm^3 mol^{-1} K, close to the expected value, in the free-ion approximation, for two isolate Pr^{3+} ($^3H_4$) ions (3.2 cm^3 mol^{-1} K) and decreases with temperature to 0.46 cm^3 mol^{-1} K. The temperature dependence of $\chi_M T$ for the [Pr_2Fe] complex is also shown at the top of Figure 6. At 290 K, the $\chi_M T$ value is approximately equal to 4.53 cm^3 mol^{-1} K, while it decreases with temperature to 1.36 cm^3 mol^{-1} K. The $\Delta\chi_M T$ vs T curve is superimposable with the $\chi_M T$ vs T curve of the [La_2Fe] complex along the whole range of temperatures indicating that no exchange interaction is active. The experimental magnetization of [Pr_2Fe] at 2 K (Figure 6 bottom) is superimposable with that of the uncorrelated spin system, corroborating that no exchange interaction is active.

(31) Sutter, J. P.; Khan, M. L.; Khan, O. *Adv. Mater.* **1999**, *11*, 863.
(32) Kahn, O. *Molecular Magnetism*; VCH: Weinheim, 1993.

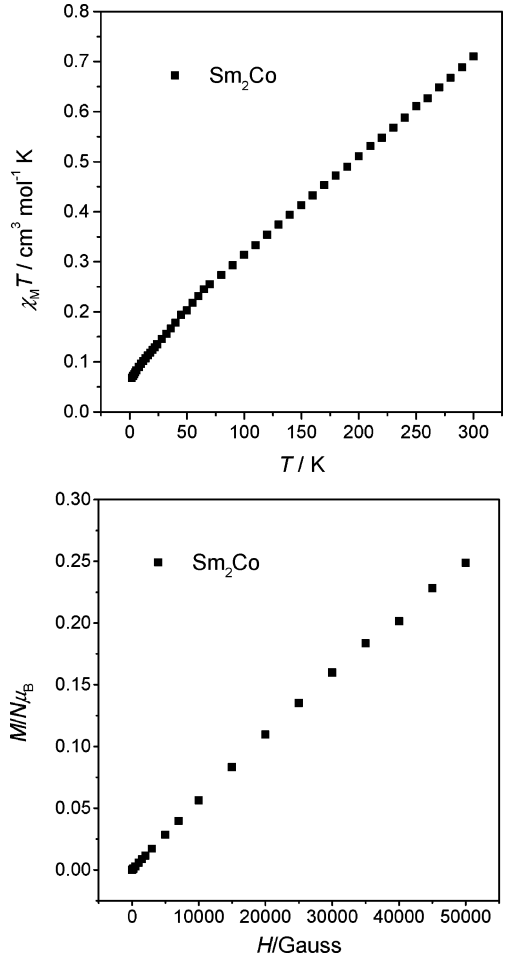

Figure 8. Thermal dependence at 0.1 T of $\chi_M^{[Sm_2Co]}T$. Bottom: magnetization vs H (2 K) of $M^{[Sm_2Co]}$.

***trans*-[Fe(CN)$_4$(μ-CN)$_2${Nd(H$_2$O)$_4$(bpy)$_2$}$_2$][Fe(CN)$_6$]·8H$_2$O (4) and *trans*-[Co(CN)$_4$ (μ-CN)$_2${Nd(H$_2$O)$_4$(bpy)$_2$}$_2$]-[Co(CN)$_6$]·8H$_2$O (7).** The temperature dependence of $\chi_M T$ for complex [Nd$_2$Co] is shown at the top of Figure 7. At 290 K, the $\chi_M T$ value is approximately equal to 3.24 cm^3 mol^{-1} K, close to the expected value, in the free-ion approximation, for two isolate Nd^{3+} ($^4I_{9/2}$) ions (3.28 cm^3 mol^{-1} K) and decreases with temperature to 1.32 cm^3 mol^{-1} K. The temperature dependence of $\chi_M T$ for the [Nd$_2$Fe] complex is also shown at the top of Figure 7. At 290 K, the $\chi_M T$ value is approximately equal to 4.58 cm^3 mol^{-1} K, while it decreases with temperature to 2.25 cm^3 mol^{-1} K. The $\Delta\chi_M T$ vs T curve is superimposable with the $\chi_M T$ vs T curve of the [La$_2$Fe] complex along the range of temperatures indicating that no exchange interaction is active. The experimental magnetization of [Nd$_2$Fe] at 2 K (Figure 7 bottom) is superimposable with that of the uncorrelated spin system, corroborating that no exchange interaction is active.

***trans*-[Co(CN)$_4$(μ-CN)$_2${Sm(H$_2$O)$_4$(bpy)$_2$}$_2$][Co(CN)$_6$]·8H$_2$O (8).** The temperature dependence of $\chi_M T$ for the [Sm$_2$Co] complex is shown at the top of Figure 8. At 290 K, the $\chi_M T$ value is approximately equal to 0.70 cm^3 mol^{-1} K, this value being inconsistent with the theoretical value of 0.00 cm^3 mol^{-1} K expected for two independent Sm^{3+} ($^7F_0$) ions. The disagreement is ascribed to the presence of thermally populated excited states, as is well known for Sm^{3+} complexes. On lowering the temperature, the $\chi_M T$ value decreases monotonically to 0.06 cm^3 mol^{-1} K. The experimental magnetization of [Sm$_2$Co] at 2 K (Figure 8 bottom) achieves only a very small value, 0.25 Nβ at 5 T. Complex **8** cannot be compared to the analogous Sm−Fe complex because this last one is not a trinuclear but a one-dimensional system already published by us.[4b]

Conclusions

Eight trinuclear [Ln$_2$Fe] and [Ln$_2$Co] complexes, involving the first elements of the lanthanide's series, have been structurally characterized and magnetically studied. All the complexes are isostructural. The synthesis in the same conditions for the other lanthanide ions with bpy and $[Fe(CN)_6]^{3-}$ or $[Co(CN)_6]^{3-}$ leads to one-dimensional complexes, some of them previously published by us,[4b] and the other are the object of Part II of this work. The changes in the structure, from trinuclear to one-dimensional systems, seem to indicate that Sm^{3+} ion is, in the first lanthanide, the limit of the trinuclear complexes when the building block is $[Fe(CN)_6]^{3+}$ and Nd^{3+} is the limit when the building block is $[Co(CN)_6]^{3-}$. The coordination polyhedron of the lanthanide ions is a distorted gyroelongated square pyramid polyhedron (GSPY-9). The magnetic interaction for the three trinuclear [Ln$_2$Fe] (Ln^{3+} = Ce, Pr, Nd) is negligible. Trying to make magneto-structural correlations has proved impossible until now due to the complexity of the 3d−4f magnetic interactions and to the few complexes reported in the bibliography with similar Ln−CN−Fe core. Part II of this work is devoted to the one-dimensional complexes obtained from the last lanthanide ions.

Acknowledgment. This work was financially supported by Spanish Government (Grant No. BQU2003-00539).

Supporting Information Available: Additional tables and crystallographic data in cif format. This material is available free of charge via the Internet at http://pubs.acs.org.

IC050648I